

www.acsanm.org Article

3D Printable Hydrogel Based on TEMPO-Oxidized Cellulose Nanofibrils and Fmoc-FF for Enhanced Biological Performance and **Cell Adhesion**

Dhanya Raveendran, Feras Dalloul, J. Benedikt Mietner, Enguerrand Barba, Shouzheng Chen, Daria Zaytseva-Zotova, Benedikt Sochor, Sarathlal Koyiloth Vayalil, Peter Müller-Buschbaum, Hanna Tiainen, Stephan V. Roth, and Julien R. G. Navarro*



Cite This: ACS Appl. Nano Mater. 2025, 8, 18571–18583

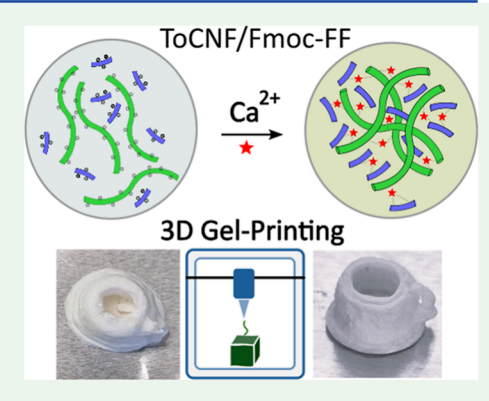


ACCESS

Metrics & More

Article Recommendations

ABSTRACT: Herein, we report a 3D printable ink made of a peptide-polysaccharide hybrid hydrogel composed of fluorenylmethyloxycarbonyl-diphenylalanine (Fmoc-FF) peptide and TEMPO-oxidized cellulose nanofibrils (ToCNF), synthesized using a pH-dependent sol-gel transition method. The ToCNF suspension is synthesized through the mechanical breakdown of a cellulose pulp using a microfluidizer, followed by its oxidation mediated with 2,2,6,6-tetramethylpiperidine-1-oxyl (TEMPO). The properties of the hybrid inks are compared in the presence (ToCNF/Fmoc-FF-Ca²⁺) and absence (ToCNF/Fmoc-FF) of the divalent cation Ca^{2+} , which acts as the cross-linker, at two optimized weight ratios (r) of ToCNF and Fmoc-FF (r = 4.5 and 6.5). The rheological measurements show that the yield strength of the ToCNF/Fmoc-FF-Ca²⁺ gel is almost double that of the hydrogel composite without Ca²⁺ ions, especially at the concentration (C) of 10 mM CaCl₂. This finding is further verified by 3D gel printing, which produced good quality prints



with the cation cross-linked hydrogel. The structural analysis by Field Emission Scanning Electron Microscopy shows that the calcium ions can cross-link the ToCNF and also enhance the self-assembly of Fmoc-FF, which leads to the formation of rigid compact nanofibers even at physiological pH. The electrostatic interaction of the positively charged Ca²⁺ ions onto the negatively charged surface carboxylate groups of ToCNF and Fmoc-FF is analyzed by zeta potential (ζ) measurements. Small-angle X-ray scattering measurements give deeper structural insights into the interaction of Fmoc-FF with ToCNF. Cell responses to the hydrogels are studied in human dermal fibroblasts (NHDFs) in a direct contact test using a live/dead assay and in extract test using Alamar Blue and lactate dehydrogenase assays. The results show that high loading of Fmoc-FF decreases cell viability, while additional cross-linking with calcium reduces this cytotoxic effect.

KEYWORDS: cellulose nanofibrils, Tempo-oxidized CNF, 3D printing, direct ink writing, hydrogels, nanocellulose, Fmoc-FF, cell adhesion

■ INTRODUCTION

In the past few decades, hydrogels have gained significant interest in numerous fields such as 3D bioprinting, tissue engineering, scaffold fabrication, drug delivery, and 3D cell culture systems, thanks to their highly tunable physical and chemical properties. 1-7 Even though 3D gel printing technology has achieved dramatic improvement in recent years, 3D printing of hydrogels prepared from low molecular weight gelators (LMWGs) is still in its way of development. Over the traditional gel materials, peptide-based self-assembled hydrogels offer many advantages, including good mechanical strength, dynamic gelation behavior, biodegradability, and large possibility for modulation by changing the peptide sequence. $^{8-11}$ Moreover, it was reported that the structural and functional properties of peptide hydrogels can easily be tuned by simply modifying the gelation kinetics or through other external stimuli. 12 For

example, the mechanical properties of the hydrogel can be changed of up to 4 orders of magnitude by changing some conditions such as temperature, peptide concentration, pH of the solution, and the addition of salt/additives/cross-linkers. 13 Therefore, the mechanical properties of the LMWGs hydrogels can be tuned and used in 3D gel printing. 12,14,15 Among the various peptidic-based systems, the fluorenylmethyloxy-carbonyl-diphenylalanine (Fmoc-FF) dipeptide is one of the most suitable candidates for hydrogel preparation. Apart from the

Received: July 16, 2025 September 4, 2025 Revised: Accepted: September 9, 2025 Published: September 16, 2025





relative cost-effectiveness and its chemical simplicity and versatility, Fmoc-FF can form hydrogels even at physiological pH, on which fibroblast 3T3 and HaCat cell lines can grow and proliferate. 16-18 Another advantage of using Fmoc-FF as a building block for hydrogel preparation is its fast kinetics of gelation, which occurs in a few minutes. 13 In the appropriate conditions, Fmoc-FF has the ability to self-assemble into a supramolecular nanostructure, which finally yields a structured three-dimensional gel. Tang et al. 16 proposed an organization model in which the Fmoc-FF peptides are arranged in an antiparallel β -sheet pattern. The Fmoc groups from alternate β sheets interlock with each other and form pairs that interact via π -stacking. These Fmoc pairs are interleaved by phenyl rings. Due to the intrinsic twist of the β -sheets, four sheets come together to create cylindrical fibrils. 19 An interesting feature of these peptide-based systems is their ability to self-assemble into a variety of functional nanostructures, 20 including spherical particles, 21 nanotubes, 22 nanoribbons, 23 or nanowires. 20

Raeburn et al.²⁴ have reported that gels formed through the solvent-triggered method outperform the mechanical properties of those created via the pH-triggered method. However, since the final pH in the solvent switch method tends to be around 4, it restricts its suitability for biological applications. One should also notice that the formation of Fmoc-FF nanowires at pH 7 is still possible, but the formed gel is not as stiff and stable. Despite their excellent mechanical properties, the processing of those Fmoc-FF gels through 3D printing application continues to pose a significant challenge due to their inherent stiffness and lack of uniformity, especially in the pH switch gelation method, which results in fragmentation during extrusion.²⁵ One potential approach to meet the required gel printing needs, or properties, is to incorporate some additional functional components within the Fmoc-FF matrix and create a hybrid gel system, thereby enhancing the physicochemical properties of the resulting material. ²⁶⁻²⁸ Gong et al. ¹⁰ in their study revealed that the introduction of polysaccharides into a peptidic system can enhance the self-assembly process and also improve the biocompatibility of the system. Xie et al. 27 showed the influence of calcium ions in the coassembly of Fmoc-FF and the alginate system that was intended for drug delivery applications.

Following this strategy, this has greatly inspired us to develop a new 3D printable hybrid peptide-polysaccharide system composed of Fmoc-FF and ToCNF.

Cellulose nanomaterials extracted from wood biomass, in this case ToCNF, are an attractive green platform and are extensively studied, notably for their biocompatibility, renewability, hydrophilicity, and good viscoelasticity, all of which are beneficial for 3D printing application. ^{29–32} Several studies have reported on the application of nanocellulose-based inks for 3D gel printing, mainly in the context of potential biomedical gels for regenerative medicine with self-healing behavior. 33,34 The pristine CNF is generally obtained through the mechanical disintegration of a cellulosic pulp by using a microfluidizer. The treatment of the obtained CNF with the 2,2,6,6-tetramethylpiperidine-1-oxyl, in combination with some sodium hypochlorite, leads to the oxidation of the C₆ primary hydroxyl functions (glucose units) into carboxylic acid groups. The oxidized fibrils carry an abundant number of negative charges onto their surface, creating an electric repulsion between the fibrils, which lead to an extremely stable suspension of ToCNF in water. 35 Moreover, structures based on ToCNF have the ability to absorb and retain significant amounts of water while creating a complex network, positioning them as a promising candidate for hydrogel

production. The hydrophilic nature of CNF, along with the electrical sensitivity of cellulose to water vapor, enables CNF structures to function as moisture sensors. ³⁶ For example, it can be used in the effective monitoring of wound moisture, which helps to maintain an adequate moist environment while supporting cell proliferation and therefore affect the wound healing time. ^{35,37–39}

The aqueous dispersion of carboxylated CNFs can display a "gel-like" consistency even at moderate concentrations, but it can easily be disrupted by high shear rates, transitioning into a flowable liquid because of its shear-thinning properties. 40 To improve the mechanical properties of ToCNF hydrogels, which have characteristics similar to those of a weak gel system, the ability of ToCNF to establish stronger ionic interactions with metal ions could be utilized. 41,42 One straightforward method for the CNF physical cross-linking is the addition of metal cations (e.g., Al³⁺, Fe³⁺, Zn²⁺, Cu²⁺, Ca²⁺) into a ToCNF suspension. The di- or trivalent metal cation can therefore interact with the negative charges of the CNF (chelating effect) and electrostatically cross-link the ToCNF. This enhances rapid cross-linking, which initiates the gelation and reinforces the network structures of the oxidized CNF-based hydrogels. It also allows the tuning of the mechanical and rheological properties of the gels by varying the cation nature and concentration.^{27,44}

In this study, our main aim is to develop a hybrid 3D printable ink made of ToCNF and Fmoc-FF and to compare the properties of the gel in the absence or presence of the divalent metal cation Ca²⁺. Here, we expect the combination network will enhance the stability of the gel due to the presence of both noncovalent and ionic interactions when compared with the Fmoc-FF or ToCNF hydrogel alone. The composite hydrogel properties and their 3D printing performance are subject to comprehensive evaluation in order to ascertain their biocompatibility and mechanical properties. The influence of the calcium ion concentration and the solid content of the gel are adjusted to investigate their effect on the mechanical properties, printability, and print fidelity. The mechanical properties are characterized through detailed rheological studies, while the gelation process and structural features were analyzed using ζ measurements and small-angle X-ray scattering (SAXS).

The cryogels, which are obtained through a freeze-drying process of the hydrogel, are evaluated in terms of their morphology. This evaluation is conducted through visual inspection and field emission scanning electron microscopy (FESEM). Biological evaluations are carried out in order to investigate the hydrogel's biological compatibility, including cell viability and cytotoxicity assays. This research demonstrates the fabrication of advanced material systems with a specific focus on their ability to maintain structural integrity and highlights their potential applications in 3D printing.

MATERIALS AND METHODS

Materials. Fmoc-Phe-Phe-OH (Fmoc-FF) was acquired from BLD Pharmatech. The dry cellulose material, elemental chlorine-free bleached softwood kraft pulp, was obtained from MERCER Stendal GmbH, Germany. The Northern bleached softwood kraft pulp sample consisted of pine (30–60%) and spruce (40–70%) according to the supplier's specifications. The material was subjected to PFI milling at a temperature of 23 °C with a relative humidity of 50%. The production of cellulose nanofibrils (CNFs) was performed by processing the softwood Kraft pulp through a Microfluidizer model M-110EH-30 from Microfluidics. The grinding degree of the pulp was determined using a Schopper—Riegler analyzer (KARL SCHÖRNER KG, Germany).

Reagents, including 2,2,6,6-tetramethylpiperidine-1-oxyl (TEMPO, 98%), hydrochloric acid (37%, HCl), ethanol (96%), sodium hydroxide (NaOH), sodium bromide (99%, NaBr), and calcium chloride dihydrate (99%, CaCl₂), were purchased from Sigma-Aldrich and employed without further purification. Sodium hypochlorite pentahydrate (minimum 40% available chlorine) was purchased from TCI EUROPE N.V. with no further purification required. The synthesis methods were conducted with Milli-Q water, previously purified to a resistivity of 0.055 μ S cm⁻¹ using a PURELAB Option-Q System.

Bovine serum albumin (BSA, cold ethanol fraction, pH 5.2, ≥96.0%), phosphate buffered saline (PBS), Dulbecco's modified Eagle's medium (DMEM), fetal bovine serum (FBS), 0.02% trypsin—EDTA solution, and propidium iodide (PI) were purchased from Sigma-Aldrich. Solution of penicillin—streptomycin and GlutaMAX supplement were obtained from Gibco. Cytotoxicity Detection Kit (LDH, Roche), CellTracker Green CMFDA dye, and AlamarBlue HS Cell Viability Reagent were from Invitrogen.

Cells and Cell Culture Conditions. Normal adult human dermal fibroblasts (NHDF) were purchased from Lonza (Basel, Switzerland). NHDFs were cultured in DMEM containing low glucose (1 g·L $^{-1}$), sodium bicarbonate (3.7 g·L $^{-1}$), 100 units·mL $^{-1}$ of penicillin, 100 μg ·mL $^{-1}$ of streptomycin, 2 mM GlutaMAX, and 10 vol % heat-inactivated FBS. NHDFs were maintained in a humidified incubator with a 5% CO $_2$ atmosphere at 37 °C. Cells were subcultured prior to reaching confluence using trypsin—EDTA solution.

Production of Cellulose Nanofibrils (CNFs). The CNF was prepared according to a previously reported procedure. ⁴⁵ Briefly, the cellulose pulp was first suspended in water and then ground to obtain a 75–80° SR (SR: Schopper–Riegler degrees, determined using the Schopper–Riegler method (DIN EN ISO 5267-1)). After that, the ground slurry was further refined with a microfluidizer under high pressure by passing the slurry several times in different chambers with orifice widths of 400 and 200 μ m (2 times, 15,000 ψ) and 200 and 100 μ m (4 times, 25,000 ψ) successively. The resulting CNF was obtained in the form of an aqueous gel with a concentration within the range of 2–3 wt %.

TEMPO-Mediated Oxidation of CNF. TEMPO-oxidized CNF (ToCNF) was prepared by TEMPO-mediated oxidation in water at pH 10 according to a previously described method. 46 According to this method, 121 g of CNF suspension (2.9 wt %) was mixed with 520 mL of distilled water, TEMPO (0.06 g, 0.39 mmol), and NaBr (0.36 g, 3.5 mmol). NaClO·5H₂O (5.88 g, 79 mmol) was then added to initiate the reaction. The reaction was made at room temperature, and the pH was kept at 10 through the addition of a 0.5 M NaOH solution over a period of 2 h. No further or slow pH changes were observed, indicating the completion of the reaction. The reaction was then quenched through the addition of 15 mL of ethanol, and the pH was lowered to 4 using a 1 M solution of HCl. The suspension was concentrated by centrifugation to give a white gel, and the supernatant was discarded. The carboxylate content of ToCNF was determined by conductometric titration using 0.05 M NaOH as the titrant. The excess salts and reagents present in the obtained ToCNF were removed through a dialysis procedure. The ToCNF was added to Thermo Scientific SnakeSkin Dialysis Tubing (10 kDa) and submerged in 3 L of distilled water. This process was repeated once, and the resulting TOCNF was concentrated by centrifugation. In order to obtain a high concentration of ToCNF, 50 mL tubes were used, and centrifugation was carried out at 20,000 rpm for 2 h. This method yielded ToCNF with a concentration in the range of 4-5 wt %.

Preparation of (a)ToCNF/Fmoc-FF Hydrogels. In this preparation method, a homogeneously dispersed solution of 0.017 g Fmoc-FF was prepared in deionized water, which was then solubilized by the dropwise addition of 1 M NaOH. It was then mixed well with 1.5 g of ToCNF (5.1 wt %) suspension using a ROTISpeed stirrer. At this stage, the pH of the gel was maintained at an alkaline pH of 10. The pH of the gel was then adjusted to 7 with a solution of HCl (0.5 M). We followed the same procedure for making different weight ratios (r) of ToCNF and Fmoc-FF.

Preparation of (b)ToCNF/Fmoc-FF-Ca²⁺ Hydrogels. The procedure was the same as that for ToCNF/Fmoc-FF hydrogels.

Once the pH was adjusted to 7, a known amount of CaCl₂ was added. To monitor the final hydrogel concentration and CaCl₂ concentration, each time fresh starting buffer solutions were made, and an exact volume of each was taken to keep track of the final concentration. We tried different concentrations of calcium ions. For example, to prepare the gels with 10 mM CaCl₂ and a solid gel content of 3.5 wt %, 0.27 mL of a solution of CaCl₂ (100 mM) was added to the ToCNF/Fmoc-FF gel. Finally, the resulting gel was mixed using a ROTISpeed stirrer and left for 2 h without disturbance. At each step of the procedure, the pH was monitored.

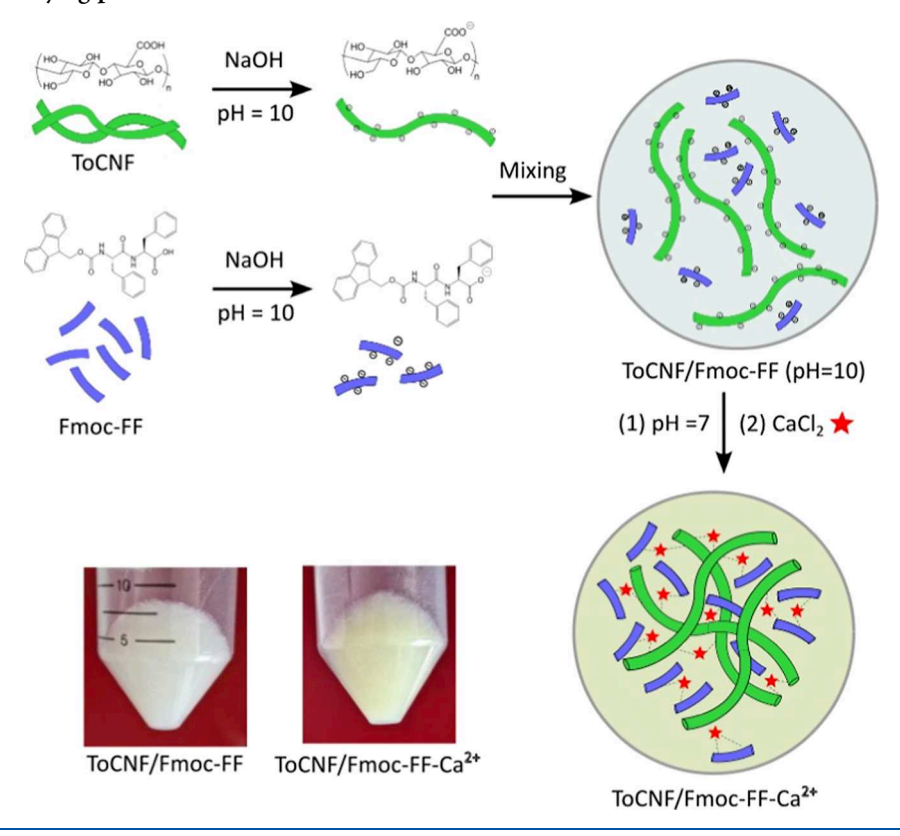
3D Printing of Hydrogels and Cryogels Production. Different models such as mug-shaped (15 mm \times 10 mm \times 10 mm) and flowershaped (16 mm \times 16 mm \times 3 mm) have been designed using Fusion360 and 3D gel printed by pneumatic extrusion using a CELLINK INKREDIBLE 3D bioprinter. A disposable gel cartridge was charged and fitted into the print head. The printability was adjusted by setting the pneumatic pressure to about 35 kPa to achieve stable and consistent extrusion through the nozzle. The gel was printed with two different conical nozzle diameters (0.58 or 0.41 mm) with a printing speed of 30 mm/s. The printed structures were stored in a fridge until they were frozen using liquid nitrogen and then freeze-dried using oil pump vacuum up to 10^{-2} mbar to obtain the relative cryogels.

Characterization Methods. Field Emission Scanning Electron Microscopy. All of the measured samples were freeze-dried to yield cryogels and mounted on sample supports using carbon tape. The sample surfaces were then coated with a 5 nm layer of Gold under an inert atmosphere with a BIORAD SC510 sputtering machine before microscopic imaging. The morphological properties of ToCNF, Fmoc-FF, and ToCNF/Fmoc-FF-Ca²⁺ composites were observed using an ultrahigh-resolution field emission scanning electron microscope (Quanta FEG Type 250, FEI Electron Optics SN:D9122, the Netherlands) at an acceleration voltage of 10 kV and high-vacuum conditions using an Everhart-Thornley Detector.

Rheology. Rheological tests were conducted on the samples using a TA Instruments AR 2000ex rheometer with Advantage v5.8.2 software. A 40 mm parallel plate configuration with a gap of 1000 μ m was employed with the gel positioned on the lower plate. A series of frequency sweeps was conducted within the range of 0.1–100 rad·s⁻¹, and a series of strain sweeps was carried out at an angular frequency of $6.28~{\rm rad\cdot s^{-1}}$ to ensure that the measurements were taken within the linear viscoelastic region (LVE). A shear stress ramp was applied to each sample, increasing the strain from 0.01 to 100 Pa. Rotational shear viscosity measurements were conducted in flow mode, with shear rates ranging from 0.01 to 2000 s⁻¹. The rheological properties were evaluated at 25 °C to ascertain the viscosity behavior of the material subsequent to 3D printing. The test sequence comprised a low shear rate of 0.01 s⁻¹ for 200 s, followed by a high shear rate of 895 s⁻¹ for 100 s and concluded with a low shear rate of 0.01 s^{-1} for another 200 s. The yield stress was determined by applying an increasing shear stress and monitoring the material's viscoelastic properties (G' and G''). The yield stress was identified at the point where the viscoelastic response decreased, indicating a transition from elastic to plastic behavior.

Synchrotron-Based Small-Angle X-ray Scattering. Small-angle Xray scattering (SAXS) measurements were conducted at beamline P03 of PETRA III at Deutsches Elektronen-Synchrotron DESY in Hamburg.⁴⁷ A beam diameter of 25 μ m, with a wavelength of λ = 0.105 nm and a sample-to-detector distance (SDD) of 5441.1 mm, was used. A PILATUS 2 M detector (Dectris, Switzerland) with a pixel size of 172 μ m was used, and each pattern was captured with an exposure time of 10 s. All data underwent a background correction. The samples were scanned over an area of $2 \times 2 \text{ mm}^2$ with a step size of 0.1 mm, each acquisition taking 1 s to minimize beam damage. Subsequent images were summed and radially integrated for data analysis, allowing for the derivation of intensity I(q) as a function of wavevector transfer q. For data analysis, SASview version 5.0.5 was utilized in conjunction with χ^2 minimization (SasView Application. Version 5. Released June 3, 2022, https://www.sasview.org/). A mask file was applied prior to integration of the 2D SAXS pattern. We used a sufficiently long cylindrical form factor to statistically analyze the radii of the Fmoc-FF and the ToCNF samples detected in the sample. The distribution of the detected

Scheme 1. Schematic Representation of Each Component, ToCNF, Fmoc-FF, and CaCl2 at pH 7 and the Interaction of ToCNF with Fmoc-FF under Varying pH Conditions and Ca²⁺ Influence



interaction between the Fmoc-FF and ToCNF structure domains was fitted by using a Gaussian distribution.

Zeta Potential (ζ). The ζ of all the samples was calculated from their electrophoretic mobilities, which were measured using a Zetasizer Nano ZS from Malvern. A laser with a wavelength of 633 nm was used and measured in a fast field reversal mode. The diluted solutions of Fmoc-FF, ToCNF, and ToCNF/Fmoc-FF in the presence and absence of Ca²⁺ ions were measured at acidic, neutral, and basic pH.

Biological Characterizations. Direct Contact Test. Dry samples were placed into wells of a 48-well plate, and 100 μ L/sample of cell suspension was added on top of the samples. Cells were seeded at a density of 3×104 cells/sample. After cell suspension was absorbed by the sample, 500 μ L/well of medium was carefully added into the wells, and cells were placed at 37 °C in a CO₂ incubator. After 24 h, old medium was aspirated, and cells were stained with 500 μ L/well of medium with 1 μ M CellTracker Green CMFDA dye (live cells) and 0.4 μ M PI (dead cells) at 37 °C for 30 min. All the samples, namely, ToCNF, Fmoc-FF, ToCNF/Fmoc-FF, and ToCNF/Fmoc-FF-Ca²⁺ (C = 10 mM), were then washed in PBS and immediately imaged using an upright CLSM microscope (Leica, Wetzlar, Germany) equipped with a 20× water objective. Confocal microscope images were processed by using ImageJ, Fiji-program.

Extract Test. Preparation of extracts: Each sample was weighed and sterilized with ultraviolet (UVC) radiation for 30 min on each side. Samples were then transferred into microtubes containing the corresponding volume of complete cell culture medium containing phenol red (extraction volume of 0.01 g⋅mL⁻¹) and incubated at 37 °C for 24 h. The next day, the extracts were visually inspected for the presence of particles/debris and color change.

Sample swelling analysis: Swollen samples were weighed out, and the mass swelling ratio was calculated using the following equation: Q = W_s/W_d , where W_s is the weight of the swollen sample after 24 h and W_d is the initial weight of the dry sample.

Cell exposure to extracts: Cells were seeded in 96-well plates at a density of 7000 cells/well and were allowed to adhere overnight. Next day, old medium was aspirated, and 100 μ L/well of undiluted extracts

as well as extracts diluted with fresh medium in 1:3 and 1:9 ratio were added to the cells before the plates were incubated at 37 °C in a CO₂ incubator. After 48 h, cell culture medium was collected from each well for analysis of acute cytotoxicity using lactate dehydrogenase (LDH) assay according to the manufacturer's recommendations with minor modification: the reaction volume was reduced from 200 to 100 μ L. For analysis of cell viability, the cells remaining in the wells were further incubated in 200 μ L/well of medium containing a 10 vol % alamarBlue HS reagent for 1.5 h, after which the fluorescence intensity was determined at an excitation/emission wavelength of 530/590 nm (BioTek Synergy HT).

Toxicity of Fmoc-FF. Cells were seeded in 96-well plates at a density of 7000 cells/well and were incubated at 37 °C in a CO2 incubator overnight. Next day, old medium was aspirated, and 200 μ L/well of 1:3 serial dilution of Fmoc-FF in fresh medium was added to the wells. Serial dilutions of Fmoc-FF were prepared in two steps: First, serial dilutions of Fmoc-FF were prepared in DMSO and then further diluted 200 times in culture medium to a final concentration of DMSO of 0.5 vol %. The highest tested concentration of Fmoc-FF was 500 μ M. NHDFs were incubated with Fmoc-FF at 37 °C in a CO₂ incubator for 24, 48, and 72 h. At each time point, acute cytotoxicity was determined using lactate dehydrogenase (LDH) assay according to the manufacturer's guidelines, and cell viability was analyzed using alamarBlue HS reagent as described in "Extract test".

Statistical Analyses. The results are presented as mean \pm standard deviation. Differences between the groups were assessed by one-way analysis of variance test with Tukey post hoc analysis using IBM SPSS Statistics 30 software. A p-value <0.05 was considered statistically significant.

RESULTS AND DISCUSSION

Cross-linked hydrogels are produced through the combination of ToCNF and Fmoc-FF nanowires triggered through the introduction of calcium cations (Ca²⁺). Following the process of defibrillation of CNF via microfluidization, the CNF has undergone a TEMPO-mediated

Table 1. Composition of Compounds and the Effect of CaCl₂ Concentration and ToCNF/Fmoc-FF Weight Ratio on Yield Strength (pH 7) and the Linear Viscoelastic Region (LVE)

material composition	weight ratio (r) of ToCNF and Fmoc-FF	$CaCl_2$ concentration (C) in (mM)	yield strength (Pa)	G'_{LVE} (Pa)	G''_{LVE} (Pa)
•Fmoc-FF		40	5.5	453	87
•ToCNF		27.4	0.4	12.46	2.58
●ToCNF/Fmoc-FF-Ca ²⁺	4.5	10	630	2727	355
ToCNF/Fmoc-FF-Ca ²⁺	4.5	4.5	125		
•ToCNF/Fmoc-FF	4.5	0	316	1226	172
●ToCNF/Fmoc-FF-Ca ²⁺	6.5	4.7	316	1107	165
 Fmoc-FF ToCNF/Fmoc-FF-Ca²⁺ (r = 6.5, C = 4.7 mM) ToCNF/Fmoc-FF (r = 4.5) 					

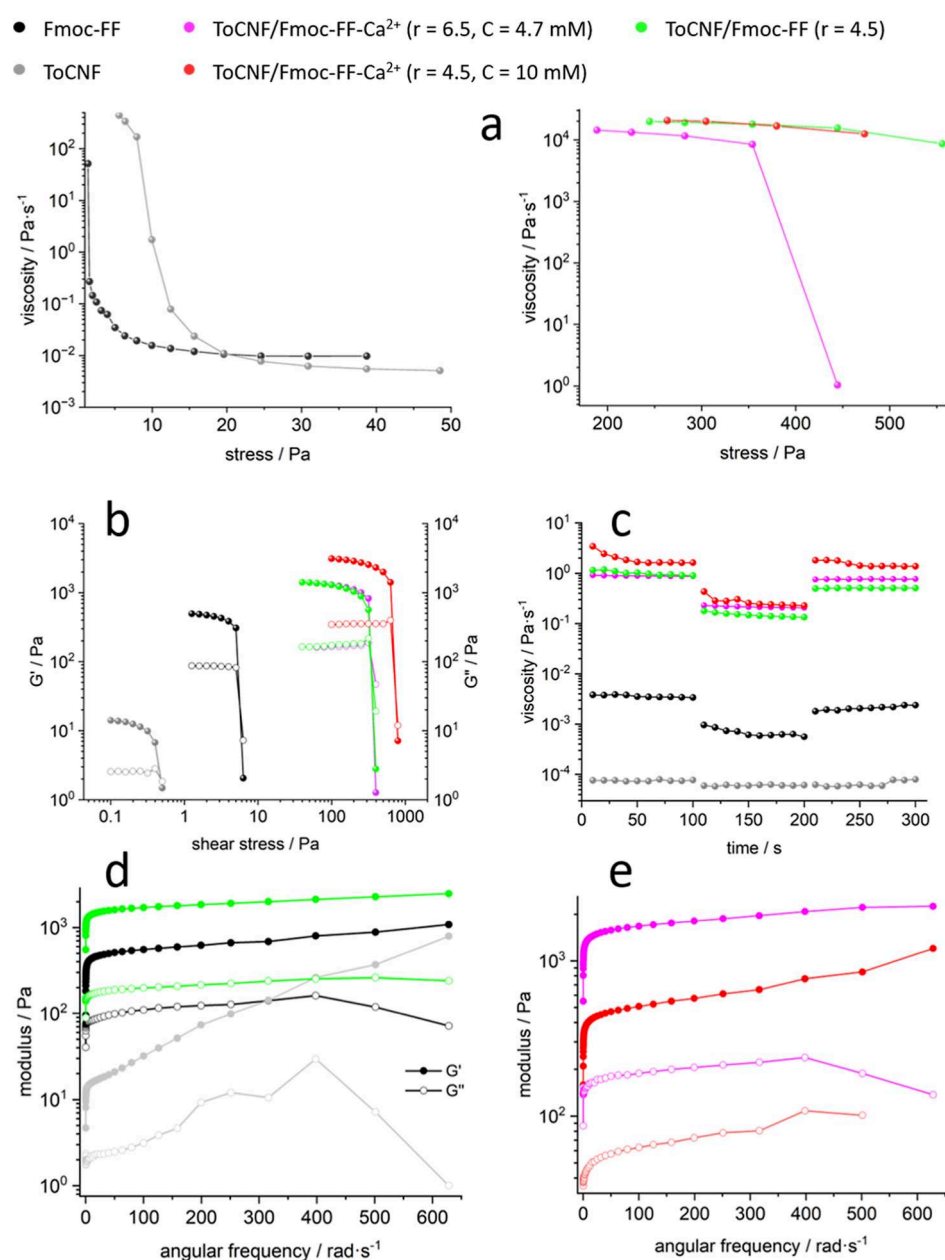


Figure 1. Graphical representation of rheological test results; colors corresponding to each sample are displayed at the top; (a) shear stress ramp data; (b) dynamic modulus under increasing stress to determine yield stress; (c) thixotropy tests with small $(200 \, \text{s}^{-1})$ and large $(800 \, \text{s}^{-1})$ pressure applied to gels; (d,e) viscoelastic (storage modulus G' and loss modulus G'') properties data measured with increasing angular frequency.

oxidation procedure as previously described in the literature. The results of the NaOH titration demonstrate that the concentration of carboxylate groups is 2.96 $\rm mmol\cdot g^{-1}$. The higher carboxylate content may be attributed to the initial defibrillation of the cellulose, resulting in an increased accessible surface area of the cellulose and, consequently, a greater interaction between the oxidant and CNF.

freshly prepared sodium chlorite $(NaClO_2)$ solution prior to the oxidation process might have contributed to minimizing the degradation of the oxidant.

Both ToCNF and Fmoc-FF have been observed to undergo a pH-dependent sol-gel transition. The transition is driven by the deprotonation and protonation of their respective acid functions

within both structures to trigger gel formation. The gel composite in question is produced by mixing the ToCNF with a Fmoc-FF solution at pH 10 (Scheme 1). When the ToCNF gel is mixed with the Fmoc-FF solution at pH 10, the -COOH groups dissociate into -COO groups under alkaline conditions, thereby increasing the hydrophilicity and electrostatic repulsion of the structure, which results in the observed improved water absorption ability. The high pH value (pH 10) is chosen to (A) solubilize the Fmoc-FF building blocks, which are present in their ionized form, and to (B) largely inhibit their selfassembly into nanostructures. After mixing the two components, i.e., the suspension containing ToCNF and the solubilized Fmoc-FF, followed by a gradual reduction in pH, induces the gelation according to the established pH switch protocol. 13,50 During this process, the fibrils come into closer proximity, as evidenced by the increased compaction that leads to the formation of a gel network.^{31,32,48,51-53} We noticed that the gel has a slightly yellowish color at elevated pH, which disappeared at pH 7. This may primarily result from the pH-induced deprotonation, conformational changes, and assembly of both cellulose nanofibrils and peptide molecules under alkaline conditions. The mixture retained a smooth appearance during stirring with no evident phase separation. The final pH of the composite is adjusted to a value of 7 by the addition of a solution of HCl, to maintain it in the physiological pH range. Here, we exploit the advantage of using Fmoc-FF and its ability to form hydrogels, even at a physiologically relevant pH value. Tang et al. 16 had investigated the impact of pH on the self-assembly process of Fmoc-FF. Their findings indicated that a decrease in pH facilitates the self-assembly of Fmoc-FF building blocks, which is associated with two noticeable pK_a shifts (approximately 6.4 and 2.2 pH units) above the theoretical pK_a value of 3.5. Corresponding to the first pK_a shift, within the pH range of 10-9.5, both protonated and unprotonated molecules begin to self-assemble into paired fibrils. As the pH decreases from 9.5 to 6.2, the surface charge of the fibers declines, leading to the formation of large, rigid aggregates due to increased lateral interactions among the fibers. Below pH 6.2 (specifically between 6.2 and 5.2), the second apparent pK_a shift is observed, resulting in further aggregation of the peptides. ¹³
In spite of their ability to form hydrogen bonds ⁵⁴ and π – π stacking

interactions, the strengths of these bonds might theoretically be insufficient for the formation of a semistiff, stable gel at this physiological pH, which is also evidenced by the rheology data. In order to overcome this situation and to enhance the electrostatic and chelation process for producing gels within physiological conditions, a divalent counterion, Ca2+ of CaCl2, is introduced to induce crosslinking of the system. Three possible cross-linkings could occur during this addition: Fmoc-FF with Fmoc-FF, ToCNF with Fmoc-FF, and ToCNF with ToCNF. This approach is inspired by previously described methods for ToCNF, as reported by Mietner et al.³⁵ and Xie et al. The requisite concentration of CaCl₂ (10 mM) enhanced the ionic cross-linking of carboxylate groups on the ToCNF. The precise concentration of calcium ions in the final hydrogel was carefully controlled, with multiple concentrations tested to study their effect on gel properties. Once within the dispersion, metal cations are capable of initiating electrostatic interactions with carboxylate groups, which exhibit negative electrical charge. This is evidenced by the change in gel transparency and its transition to a turbid state (Scheme 1).

ToCNF/Fmoc-FF-Ca²⁺ hydrogel was thoroughly mixed and left in suspension for a minimum of two h to ensure complete diffusion of the cations into the preformed gels. The resulting gel composite with a solid content of 3.5 wt % was observed to be macroscopically homogeneous and exhibited a hazy/cloudy appearance, in comparison to the starting gels or gels prepared from Fmoc-FF.

Rheology. To investigate the distinctive characteristics of each gel and the intermolecular interactions they exhibit, along with their suitability for extrusion gel printing, a series of rheological tests were conducted on each sample. To ensure consistency, the gels are prepared using a standardized methodology, with identical preparation techniques, overall concentrations, and pH values. The composition of each sample is presented in Table 1.

The outcomes of these tests are presented in Figure 1. The figure depicts a shear stress ramp, an effective method to assess the behavior of

gels under shear stress—such as during extrusion (3D printing)—to determine whether the gels exhibit shear-thinning behavior.

Figure 1a (left) shows the logarithmic curves of Fmoc-FF (black) and ToCNF (gray) gels. The Fmoc-FF gel exhibits relatively low viscosities and low yield stress (intersection of both tangents: plateau and viscosity drop). 55 Fmoc-FF demonstrates a pronounced decline in viscosity upon reaching a critical stress level, indicative of pronounced shear thinning, whereas ToCNF exhibits a more gradual decline, corresponding to a more robust structure. This difference may be attributed to the longer polymer chains derived from the cellulose structure. The remaining portion of the spectrum is displayed on the right-hand side. The shear-thinning behavior is observed for the ToCNF/Fmoc-FF and the ToCNF/Fmoc-FF-Ca²⁺ samples at higher shear stress, also with a notable large increase in viscosity (if compared to ToCNF or Fmoc-FF alone). This finding indicates the formation of a highly interconnected network between Fmoc-FF and ToCNF, resulting from their coordination alongside with the Ca²⁺ counterion. The decrease in viscosity, while increasing the stress, is observed to be more gradual, exhibiting a comparatively stronger internal structure in comparison to each individual component. However, changing the weight ratio r from 6.5 to 4.5, which means an increase of Fmoc-FF content in the composite gels, results in an increase of the composite viscosity. In both cases (ratio 4.5), with or without the presence of Ca²⁺, a consistent shear-thinning behavior is observed with an increase in stress.

Figure 1b displays the plots of the storage modulus (G') and loss modulus (G'') while increasing the shear stress, in order to calculate the yield stress. The lowest initial moduli are exhibited by ToCNF, which yields at very low stress. The Fmoc-FF sample displays a comparatively more elevated value, despite the fact that it still remains within an overall low range. For the composites ToCNF/Fmoc-FF-Ca²⁺ (r = 6.5, C = 4.7 mM) and ToCNF/Fmoc-FF (r = 4.5), a relatively notable increase in yield strength is observed, accompanied by markedly elevated dynamic moduli. The observed increase of approximately 58× in comparison to the individual components serves as evidence to confirm the formation of a highly cross-linked and robust structure. The increase in Fmoc-FF content in the composite highlights its significance impact, as even in the absence of the Ca²⁺ counterion, it is capable of yielding to a similar extent as ToCNF/Fmoc-FF-Ca²⁺ (r = 6.5, C = 4.7mM). With the highest initial moduli, ToCNF/Fmoc-FF-Ca²⁺ (r = 4.5, C = 10 mM) yields at the highest stress, reflecting the strongest internal structure among the samples. It can be attributed to the addition of Ca²⁺, which plays a role in the cross-linking.

Figure 1c illustrates the thixotropic behavior of the various gels. The gels were subjected to a high shear rate for a period of time to finally return to a low shear rate. The observed behavior of all samples is suitable for 3D printing applications, as evidenced by the recovery of the initial viscosity while removing the shear stress force.

Figure 1d,e shows the storage (G') and loss (G'') moduli of the gels as a function of the angular frequency. The analysis reveals their viscoelastic behavior. ToCNF displays a complex response, with an increase in G' and a decrease in G'' at higher frequencies, an indication of the presence of structural instability. ToCNF/Fmoc-FF (r=4.5) and ToCNF/Fmoc-FF-Ca²⁺ (r=6.5, C=4.7 mM) samples exhibit stable values with minimal fluctuations at higher frequencies, indicating uniform viscous behavior. The ToCNF/Fmoc-FF-Ca²⁺ (r=4.5, C=10 mM) sample with a solid content of 3.5 wt % demonstrates the highest and most stable values, exhibiting the strongest and most robust rheological response across the frequency range.

Zeta Potential Measurements. The ζ measurement was used to determine the surface charge present onto the ToCNF, the Fmoc-FF, and the composite (ToCNF/Fmoc-FF nanowire).

The ζ is an important parameter, as it determines the stability of the suspension relative to the pH. A high positive, or negative, absolute ζ implies a stable dispersion due to the strong electrostatic repulsion between the particles. On the other hand, a low absolute ζ could lead to the formation of aggregates. Fmoc-FF molecules can be self-assembled into nanowires within a pH range of 6–8 and are stable until pH 10. At pH higher than 10, hydrolyses can occur. Therefore, in

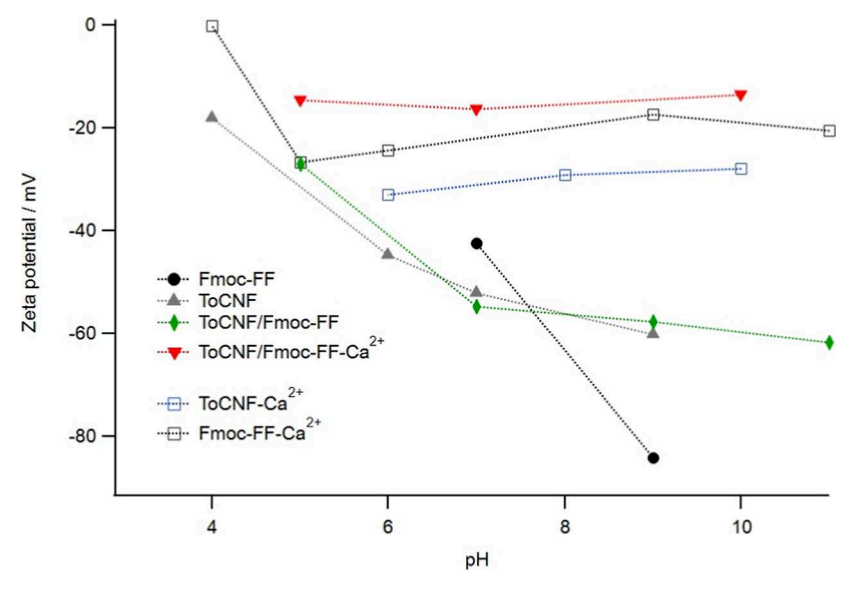


Figure 2. Zeta potential of all the suspensions at different pH values.

this study, it is relevant to consider the ζ of Fmoc-FF only within the pH range of 6–10. The results are listed in Figure 2.

Interestingly, a jump of the ζ values was observed for Fmoc-FF from around -40 to -90 mV, when the pH was increased from 6 to 10. A similar trend was also observed for ToCNF, with the shift in ζ values, approximately from -44 to -60 mV within the same pH range. This may be due to the fact that carboxylic groups, which are present in both ToCNF and Fmoc-FF, undergo protonation at low pH and deprotonation at higher pH, making them stable in their suspensions and their surface charge pH-dependent. ⁵⁸

As shown in Figure 2, the negative ζ values of ToCNF-Ca²⁺ and Fmoc-FF-Ca²⁺ decrease in magnitude within the pH range of 6–10, approximately from –33 to –28 mV and –24 to –17 mV, respectively, due to the introduction of Ca²⁺ ions into the suspension. The observation indicates effective masking of the surface charges by divalent cations, which are able to form ionic cross-links between the carboxylate groups. ⁵⁹ This is consistent with the ζ values of the hybrid composites ToCNF/Fmoc-FF and ToCNF/Fmoc-FF-Ca²⁺, which are approximately from –40 to –58 mV and from –16 to –13 mV, respectively. These results clearly demonstrate the effect of calciummediated cross-linking and the intertwining of Fmoc-FF nanowires with ToCNF nanofibrils.

Morphological Analysis Using Field Emission Scanning Electron Microscopy. The samples were characterized by using field emission scanning electron microscopy (FESEM). The resulting FESEM images are presented in Figure 3. Prior to oxidation, the initial unmodified CNF sample (Figure 3a) exhibited extensive fibril agglomeration, with only large fibril aggregates recognizable. Attributed to the strong hydrogen bonding network inherent in cellulose nanofibrils, this characteristic is often observed and promotes the fibril—fibril interaction and aggregation. 60,61

The image of the ToCNF sample (Figure 3b) shows a clear decrease in fibril agglomeration, and large fibril aggregates can no longer be observed. This defibrillation effect is attributed to the oxidation of the CNF by TEMPO-mediated oxidation, which imparts a negative charge on the fibrils, thereby enhancing electrostatic repulsion and reducing fibril—fibril interactions. ^{33,62} The morphological analysis of Fmoc-FF gels, both with and without calcium ions (Ca²⁺), reveals distinct structural characteristics. Fmoc-FF gel formed in the absence of Ca²⁺ ions a loosely packed and porous structure (Figure 3c), comprising a network of entangled nanowires with significant voids. In contrast, the Fmoc-FF gel formed in the presence of calcium ions exhibits a denser and more compact structure, characterized by a material with a smoother wrinkled surface, as shown in Figure 3d. This indicates that the ionic interactions and cross-linking facilitated by the calcium ions results in a more stable structure. The increased density and reduced

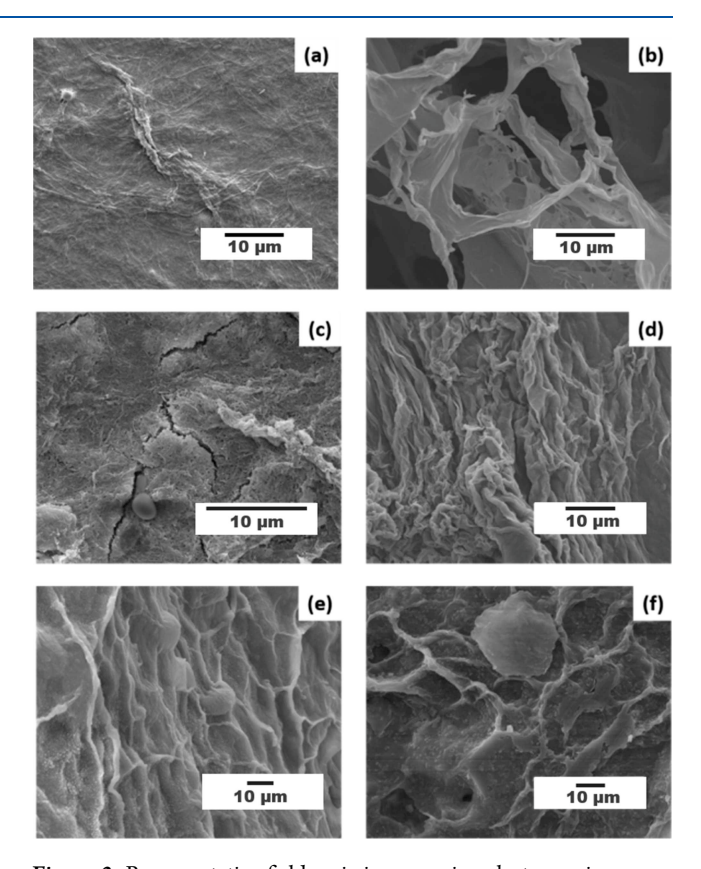


Figure 3. Representative field emission scanning electron microscopy (FESEM) images of (a) unmodified CNF; (b) ToCNF; (c) Fmoc-FF; (d) Fmoc-FF-Ca²⁺; (e) ToCNF/Fmoc-FF (r = 4.5); and (f) ToCNF/Fmoc-FF-Ca²⁺ (r = 4.5, C = 10 mM).

porosity observed in the Ca²⁺-gelated sample indicate that it is a more mechanically stable and robust hydrogel, which is consistent with the role of divalent cations in promoting gelation through electrostatic interactions.²⁷

Two distinct composite specimens were prepared through the mixing of ToCNF with Fmoc-FF, in the presence or absence of Ca²⁺ counterions. The resulting images are displayed in Figure 3e,f. In the absence of Ca²⁺ (ToCNF/Fmoc-FF), the fibrils are effectively dispersed due to the strong electrostatic repulsion between the

negatively charged nanofibrils. This leads to the creation of a network that is more homogeneous and exhibits a more uniform appearance. In contrast, the composite comprising Ca^{2+} (ToCNF/Fmoc-FF-Ca $^{2+}$) demonstrated a reduction in the extent of electrostatic repulsion. This results in the aggregation of the nanofibrils and the formation of denser and more compact structures. The formation of these aggregates results in a material that is more clustered and uneven in appearance.

Synchrotron-Based Small-Angle X-ray Scattering (SAXS). In order to deepen the understanding of the nanostructure of the materials, a series of SAXS measurements is performed. SAXS experiments are carried out to characterize the ToCNF, the Fmoc-FF, and the ToCNF/Fmoc-FF with and without the presence of Ca²⁺. All data are background corrected. We use the model based on double cylinders with a Gaussian size distribution to accurately represent and analyze the complex multiscale nanostructures observed in the hydrogels. This model allows us to disentangle the scattering contributions from individual nanofibrils and their larger assemblies (bundles) or voids, leading to a more precise understanding of the underlying architecture and material properties.

SAXS data of the ToCNF hydrogel (Figure 4a) reveal a hierarchical nanostructure of cellulose nanofibrils, with isolated fibrils (9 \pm 1 nm

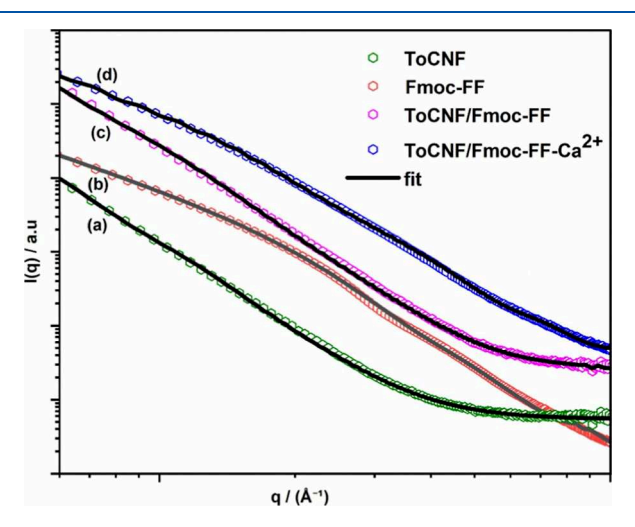


Figure 4. 1D-SAXS curves and corresponding fits of air-dried samples: (a) ToCNF (green), (b) Fmoc-FF (red), (c) ToCNF/Fmoc-FF (magenta), and (d) ToCNF/Fmoc-FF-Ca²⁺ (r = 4.5, C = 10 mM) (blue).

radius) forming elongated structures around 380 ± 28 nm in length and agglomerates or voids (35 ± 8 nm radius) extending about 450 ± 50 nm. Similarly, the Fmoc-FF hydrogel (Figure 4b) also shows two identifiable cylindrical nanostructures, with small cylinders (26 ± 1 nm radius, 18.4 ± 1 nm length) and larger cylindrical features (50 ± 1 nm radius, 10 ± 1 nm length), contributing to the three-dimensional structure. Additionally, there appears a new Gaussian contribution corresponding to a characteristic length scale of about 10 ± 1 nm. This finding further indicates the presence of ordered coil structures within the cylinders, suggesting that the molecules may form coil-like arrangements on this nanoscale.

When the SAXS data of the ToCNF/Fmoc-FF (Figure 4c) composite are compared with that of pure ToCNF, the individual fibril dimensions (radius 9 \pm 1 nm, length 330 \pm 200 nm) remain consistent across both samples. Similarly, the formation of bundles with comparable sizes (radius 35.5 \pm 3 nm, length 480 \pm 30 nm) indicates that the hierarchical architecture is preserved in the composite. The observed variations in the distribution and the associated error margins suggest that peptide incorporation may subtly influence the packing and organization of the network, potentially leading to a more ordered structure. The appearance of a broad structural feature, revealed by the Gaussian band at around 7.1 \pm 2 nm, remains aligned with the structural motifs observed in the pure Fmoc-FF hydrogel. This

observation indicates the presence of a regular, periodic structural element associated with Fmoc-FF molecules. These hypotheses are further supported by FESEM images (Figure 3).

When we compare the ToCNF/Fmoc-FF to ToCNF/Fmoc-FF-Ca²⁺ sample (Figure 4d), the fibril radius slightly decreases from ~9 to ~6 nm, suggesting that calcium ions may enhance tighter packing or induce partial compaction of the individual fibrils. In addition, the significant increase in the bundle radius from \sim 35.5 to \sim 75.5 nm and decrease in length from ~480 to ~318 nm indicate that calcium ions promote the aggregation by cross-linking into thicker fibrillar assemblies, possibly leading to more robust, denser network domains, as seen in FESEM images (Figure 3f). There are two Gaussian contributions in a calcium cross-linked composite hydrogel, one at ~209 nm, reflecting the emergence of broad, long-range periodicities or network mesh sizes likely linked to the cross-linking-induced hierarchical organization. The other band is at ~9 nm, which is consistent with the size of coil structures seen in previous data, indicating the persistence of molecular or local ordering motifs despite cross-linking.

3D Gel Printing. Different complex 3D shapes, such as mug and flower, are successfully printed using the final composites ToCNF/Fmoc-FF and ToCNF/Fmoc-FF-Ca²⁺ using a 0.58 mm nozzle, as depicted in Figure 5a-c. It has already been reported⁶³ that, within a dry matter content range of 1-5 wt % in the gel-ink, the shear-thinning rheological behavior and viscoelastic properties of the ToCNF facilitated the continuous extrusion of hydrogel filaments, which appeared to be true in our case as well, where the concentration of ToCNF is \sim 2.7 wt %. The negatively charged carboxylate ($-COO^-$) groups on CNF fibrils allow compressive stiffness and shape fidelity of the printed inks, which results in a continuous extrusion of the hydrogel filament. The strength of the gel was further increased by the inherent rigidity of the Fmoc-FF in ToCNF/Fmoc-FF hydrogel. From the rheological data, we choose ToCNF/Fmoc-FF-Ca²⁺ (r = 4.5, C = 10mM), with a solid content of 3.5 wt % as the suitable candidate for printing, which exhibits the most robust rheological response (consistent shear thinning and uniform viscosity). As anticipated, calcium-mediated cross-linking improved the structural stability of the complex geometries. It is well evident from the quality of the freezedried 3D prints (Figure 5d-f) that the introduction of calcium ions has significantly improved the interlayer bonding between the 3D-printed ToCNF/Fmoc-FF-Ca²⁺ hydrogel.⁶⁴

Among the various factors, mixing time of the gel is also an important parameter which can affect its homogeneity and the quality of the 3D-printed structures. ^{65,66} Even though we tried various techniques, we found that mixing the gel with an agitator ROTISpeed prior to printing for 5 min greatly reduced the clogging of nozzles and improved the print quality. This presents a high potential for further exploration to develop novel gels with innovative features. The freeze-dried samples which are shown in Figure 5d–f show that the new composite hydrogel can provide high potential, with robust mechanical properties.

Biological Studies. Next, we investigated the cell responses to the hydrogels. As the hydrogels were intended for use as wound dressings, human dermal fibroblasts (NHDFs) are chosen as a model cell type due to their essential role in wound healing. Moreover, these cells are of particular relevance for testing of hydrogels functionalized with Fmoc-FF, as it has been demonstrated that fibroblasts can be more sensitive to Fmoc-FF hydrogels than other cell types.⁶⁷

First, NHDFs were cultured directly on the hydrogels for 24 h (Figure 6a). Although we observed that cells were distributed throughout the hydrogels, a live/dead analysis revealed that fibroblasts retain high viability only on the ToCNF gels. A decrease in cell viability is notably more pronounced on the ToCNF/Fmoc-FF gels, where most of the cells appeared dead.

To explore why viability of cells grown on Fmoc-FF-functionalized gels was low, we further analyzed the toxicity of the extracts obtained from the gels (Figure 6b,c). Similar to observations from the direct contact test, undiluted extracts from the ToCNF gels did not affect the viability of fibroblasts, whereas all gels containing Fmoc-FF decreased cell viability to less than 50% (Figure 6b). The cells release high concentrations of LDH, indicating damage to the cell plasma

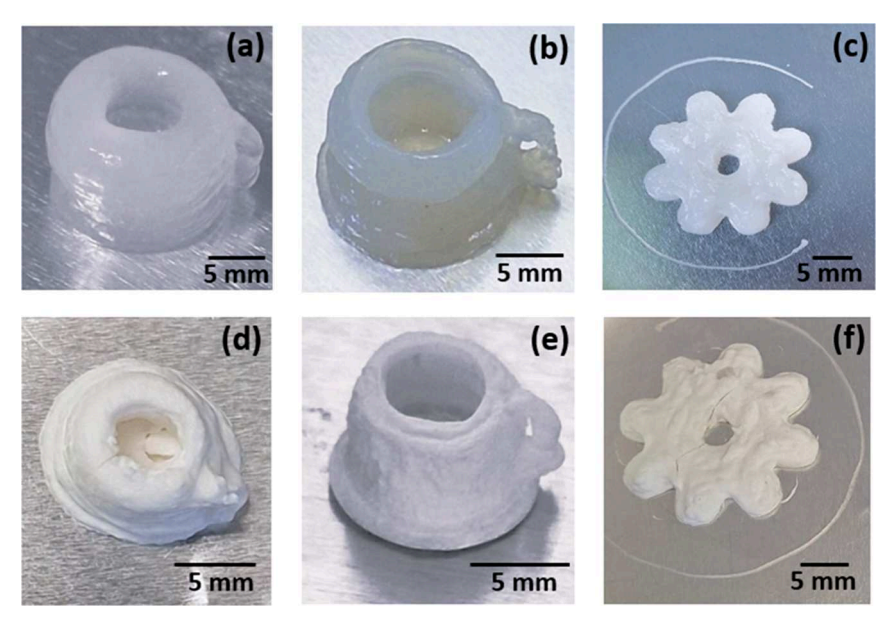


Figure 5. Pictures of 3D gel printed models: mug-shaped ($15 \times 10 \times 10 \text{ mm}$), flower-shaped ($16 \times 16 \times 3 \text{ mm}$). (a) ToCNF/Fmoc-FF (r = 4.5), (b,c) ToCNF/Fmoc-FF-Ca²⁺ (r = 4.5, C = 10 mM) samples (above) and corresponding freeze-dried samples, (d) ToCNF/Fmoc-FF (r = 4.5), and (e,f) ToCNF/Fmoc-FF-Ca²⁺ (r = 4.5, C = 10 mM) (below).

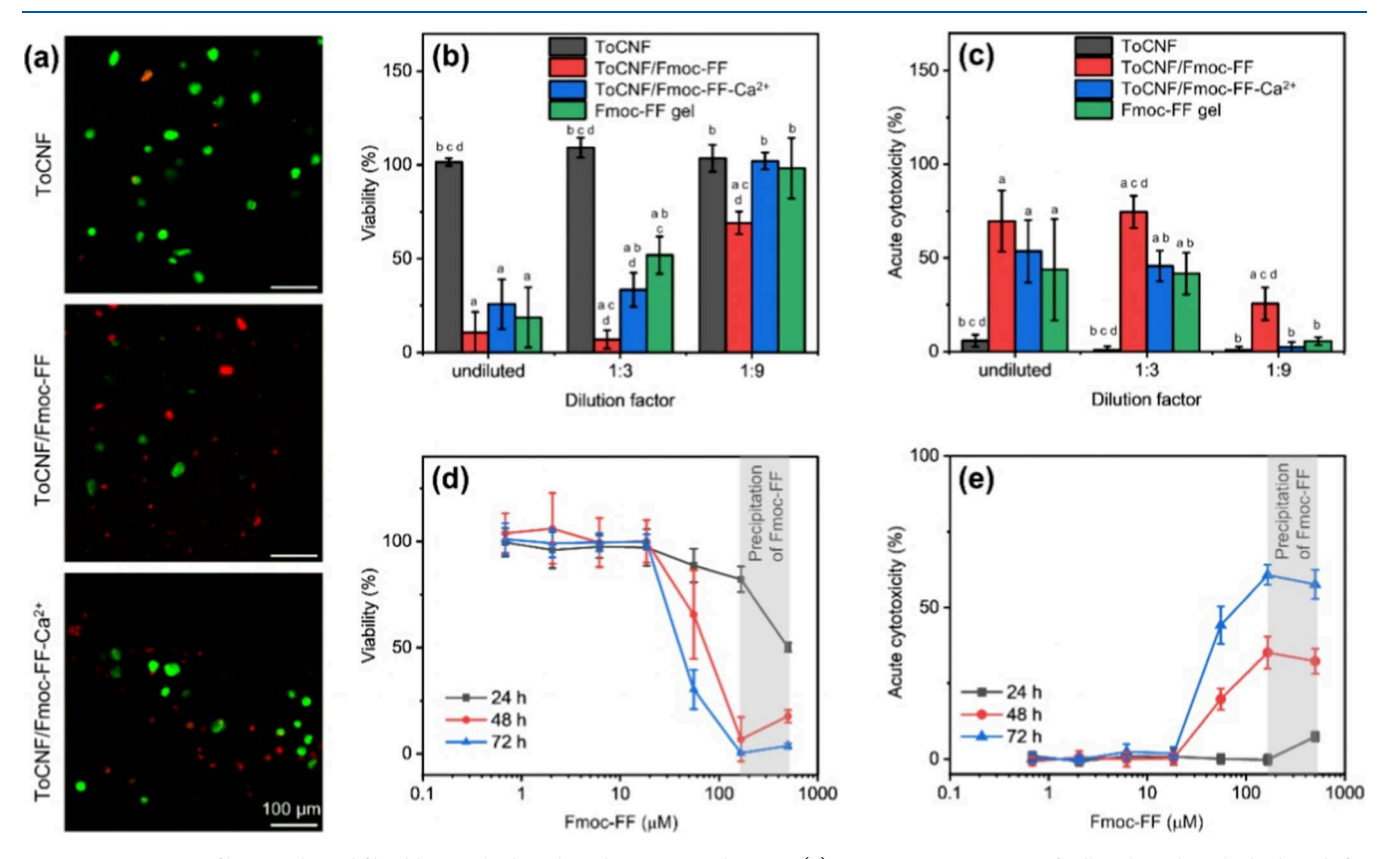


Figure 6. Response of human dermal fibroblasts to hydrogels and Fmoc-FF substance. (a) Representative images of cells cultured on the hydrogels for 24 h. Live and dead cells were labeled with CellTracker (green) and propidium iodide (red), respectively. (b,c) Cell viability (b) and acute cytotoxicity (c) after 48 h exposure to hydrogel extracts. Letters denote statistically significant differences (p value < 0.05) between bars within the same dilution. Mean \pm standard deviation, n = 4 - 6/group. (d,e) Dose—response curves of cell viability (d) and acute cytotoxicity (e) after treatment with free Fmoc-FF for 24, 48, and 72 h. Gray area indicates concentrations at which Fmoc-FF precipitate was visibly formed. Mean \pm standard deviation (n = 3).

membrane (Figure 6c), which is in agreement with previous reports showing that cells exposed to Fmoc-FF hydrogel leachate undergo necrotic cell death.⁶⁷ The greatest decrease in the cell viability was observed for the ToCNF/Fmoc-FF gel. The gels based solely on Fmoc-

FF were found to be less cytotoxic compared to the ToCNF/Fmoc-FF gel, contrary to our expectations.

To determine whether the observed toxicity could be attributed to Fmoc-FF itself, we tested the fibroblasts' response to Fmoc-FF substance. As can be seen from Figure 6d,e, cell viability decreased in

a time- and dose-dependent manner after treatment with Fmoc-FF. The half-maximal inhibitory concentrations (IC50) were 473 \pm 154, 85 \pm 37, and $64 \pm 36 \,\mu\text{M}$ after 24, 48, and 72 h, respectively. It is noteworthy that Fmoc-FF precipitated at higher tested concentrations in culture medium (>100 μ M), which is in agreement with previous reports.⁶ The precipitate that formed partially covered the cell monolayer, potentially contributing to the observed decrease in cell viability. The tested gels contained Fmoc-FF at a 14 mM concentration exceeding IC50; hence, we hypothesize that the observed cytotoxicity can be partially attributed to a high amount of Fmoc-FF release over time. Martin et al.⁶⁹ have reported in their study that higher concentrations (>0.1% (w/v) or >2.1 mM) of Fmoc-FF are well beyond the limit of ordinary cytotoxicity studies (around 0.05-0.5 mM), and some cell toxicity can be seen. According to them, the toxicity maybe due to the salts present in the cell culture media, which are disturbing the selfassembly that is observed in the fibers, resulting in smaller aggregates that most likely interact with the cell membrane.

In the experiments with extracts, we also tested gel swelling and change in pH of culture medium after 24 h incubation with the gels (Figure 7). Notably, when ToCNF/Fmoc-FF gels were submerged in

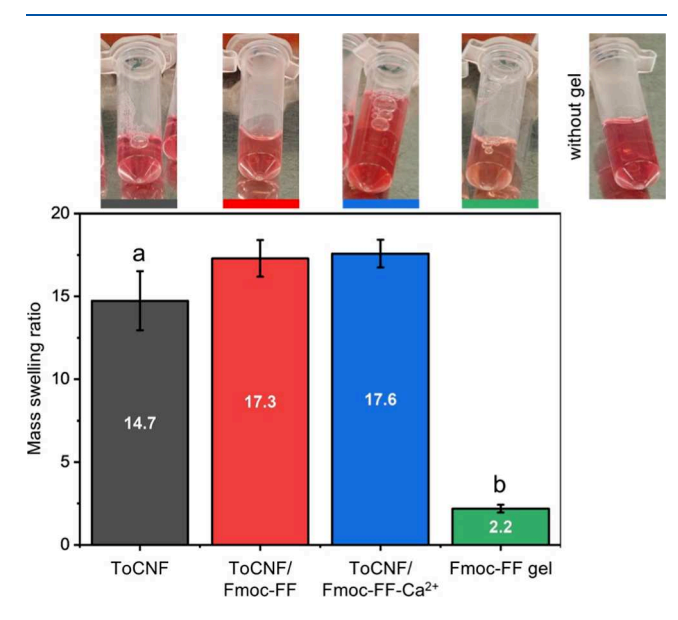


Figure 7. Swelling of hydrogels after incubation in cell culture medium for 24 h. Mean ± standard deviation, 4–6 hydrogels/group. The letter "a" denotes statistically significant differences (p value < 0.01) between ToCNF gels and ToCNF/Fmoc-FF gels as well as ToCNF/Fmoc-FF- $Ca^{2+}(C = 10 \text{ mM})$ gels. The letter "b" was used to indicate significant difference between Fmoc-FF gels and all other hydrogels (p value < 0.001). Top panel shows changes in the color of cell culture medium after 24 h incubation with the hydrogels. Cell culture medium contained a pH indicator phenol red. The photographs are arranged in the same order as the bars on the histogram. The photograph on the right shows control medium without hydrogel.

culture medium, the color of the medium around the samples changed to orange-yellow, indicating a drop in pH. After microtubes were flipped up and down, the medium restored its color to the initial redpink. After 24 h extraction, the culture medium in this group had a color different from the control sample, indicating a decrease in pH. This effect was less pronounced for ToCNF/Fmoc-FF-Ca²⁺(C = 10 mM) gels. The most significant pH shift was observed for Fmoc-FF gels, while no change in color was noted for ToCNF gels. It should also be noted that the ToCNF/Fmoc-FF and ToCNF/Fmoc-FF-Ca²⁺(C = 10mM) gels exhibited comparable swelling, which was larger than that of ToCNF gels.

Taken together, these results suggest that Fmoc-FF may be released from the gels into culture medium and thus may be a factor causing cytotoxicity. However, Fmoc-FF release alone cannot fully explain why the highest cytotoxicity was observed in the ToCNF/Fmoc-FF group rather than in Fmoc-FF gels.

In this case, we therefore assume that the presence of the ToCNF can affect the self-assembly process of the Fmoc-FF nanowires, during the formation of the ToCNF/Fmoc-FF gel composite, which in turn makes more Fmoc-FF moieties available to interact with the cell. It is also observed that the toxicity caused by $ToCNF/Fmoc-FF-Ca^{2+}$ (C = 10mM) is less pronounced and the cells are more viable compared to the hydrogel composite without calcium ions. This can be explained by the fact that the surface carboxyl groups of ToCNF are cross-linked by calcium ions, which also facilitate the self-assembly of Fmoc-FF molecules into their nanowire structures via noncovalent interactions, as the negative charges of the carboxyl groups are reduced by the calcium ions. Thus, calcium ions acts as an inducer to assemble the composite hydrogel, making it more stable and helps to immobilize the Fmoc-FF which in turn can lower the amount of Fmoc-FF released into the cell culture medium. This assumption correlates well with the ζ measurements, where there is a reduction in the net surface charge of the gels in the presence of divalent cations. Similar results were reported by Nguyen et al.,⁷⁰ where the addition of ToCNF to a cationic polyelectrolyte hydrogel showed good cell viability toward L929 and MC3T3-E1 cells. They have reported that the improved biocompatibility was due to the combination of positively charged chitosan and negatively charged ToCNF, creating differences in the gel surface.

CONCLUSIONS

In summary, we developed a series of hybrid gels made of ToCNF and Fmoc-FF, with and without the presence of a cationic calcium cross-linker. The mechanical properties of the gels are evaluated through rheology, and their suitability for 3D printing is also assessed. The viscoelastic and shear-thinning behavior show the better response for the ToCNF/Fmoc-FF-Ca²⁺ composite with a weight ratio of 4.5, 10 mM Ca²⁺, and a solid content of 3.5 wt %, which is also reflected in the quality of 3D prints. The effect of calcium ion cross-linking and intertwining of Fmoc-FF with ToCNF are further evidenced by zeta potential analysis. Differences in the structures of the individual ToCNF and Fmoc-FF gels as well as the hybrid composites are verified by FESEM analysis. SAXS analysis demonstrates the presence of physical cross-linking between ToCNF and Fmoc-FF moieties, which is facilitated by calcium ions. Cellular studies indicate that higher concentrations of Fmoc-FF in the gels decrease cell viability and increase toxicity. Based on these observations, we conclude that considerations of Fmoc-FF concentration and calcium cross-linking are crucial for the development of multifunctional hybrid hydrogels suitable for 3D printing and biological applications.

AUTHOR INFORMATION

Corresponding Author

Julien R. G. Navarro – Institute of Wood Science, Universität Hamburg, 22885 Barsbüttel, Germany; oorcid.org/0000-0001-8791-6190; Email: julien.navarro@uni-hamburg.de

Authors

Dhanya Raveendran - Institute of Wood Science, Universität Hamburg, 22885 Barsbüttel, Germany

Feras Dalloul - Institute of Wood Science, Universität Hamburg, 22885 Barsbüttel, Germany

J. Benedikt Mietner – Institute of Wood Science, Universität Hamburg, 22885 Barsbüttel, Germany

Enguerrand Barba - Institute of Wood Science, Universität Hamburg, 22885 Barsbüttel, Germany

Shouzheng Chen – Deutsches Elektronen-Synchrotron DESY, 22607 Hamburg, Germany; TUM School of Natural Sciences,

- Department of Physics, Chair for Functional Materials, Technical University of Munich, 85748 Garching, Germany
- Daria Zaytseva-Zotova Department of Biomaterials, Institute of Clinical Dentistry, University of Oslo, 0317 Oslo, Norway; orcid.org/0000-0002-5385-8399
- Benedikt Sochor Deutsches Elektronen-Synchrotron DESY, 22607 Hamburg, Germany; Advanced Light Source, Lawrence Berkeley National Laboratory, Berkeley, California 94720, United States
- Sarathlal Koyiloth Vayalil Deutsches Elektronen-Synchrotron DESY, 22607 Hamburg, Germany; Applied Science Cluster, UPES, Dehradun, Uttarakhand 248007, India; orcid.org/0000-0003-3483-3310
- Peter Müller-Buschbaum TUM School of Natural Sciences, Department of Physics, Chair for Functional Materials, Technical University of Munich, 85748 Garching, Germany; orcid.org/0000-0002-9566-6088
- Hanna Tiainen Department of Biomaterials, Institute of Clinical Dentistry, University of Oslo, 0317 Oslo, Norway; orcid.org/0000-0003-2757-6213
- Stephan V. Roth Deutsches Elektronen-Synchrotron DESY, 22607 Hamburg, Germany; Department of Fibre and Polymer Technology, KTH Royal Institute of Technology, 10044 Stockholm, Sweden

Complete contact information is available at: https://pubs.acs.org/10.1021/acsanm.5c03356

Author Contributions

The manuscript was written through the contributions of all authors. All authors have approved the final version of the manuscript.

Funding

We would like to express our thanks to the Fachagentur Nachwachsende Rohstoffe e.V. (FNR/BMEL, HolzMat3D project, number 2220HV024X) for their financial support. P.M.B acknowledges funding by DFG via International Research Training Group 2022 Alberta/Technical University of Munich International Graduate School for Environmentally Responsible Functional Hybrid Materials (ATUMS).

Notes

The authors declare no competing financial interest.

ACKNOWLEDGMENTS

We would like to thank the Thünen Institute for enabling us to make the rheology measurements. The authors also acknowledge Dr. Andrea Olbrich for the FESEM analysis. We acknowledge DESY (Hamburg, Germany), a member of the Helmholtz Association HGF, for the provision of experimental facilities. Part of this research was carried out at PETRA III, and we would like to thank Jan Rubeck for assistance in using beamline P03. Beamtime was allocated for proposal I-20230937.

REFERENCES

- (1) Mandal, M.; Deka, A. Cellulose-Based Hydrogels for Biosensing Applications. In *Cellulose-Based Hydrogells*; Elsevier, 2025; pp 281–306.
- (2) Sharma, A.; Kaur, B.; Sunaina; Kaur, G.; Tuteja, S. K.; Kumar, S. Cellulose-Based Hydrogels in Cancer Diagnostic and Therapy. In *Cellulose-Based Hydrogells*; Elsevier, 2025; pp 307—325.
- (3) Mo, Q.; Huang, L.; Sheng, Y.; Wei, Z.; Zhang, S.; Li, Y.; Wang, X.; Wang, Y.; Lu, X.; Huang, C.; Duan, Q.; Xue, M. Crosslinking Strategy and Promotion Role of Cellulose as a Composite Hydrogel Component

- for Three-Dimensional Printing A Review. Food Hydrocolloids 2024, 154, 110079.
- (4) Karvinen, J.; Kellomäki, M. 3D-Bioprinting of Self-Healing Hydrogels. Eur. Polym. J. 2024, 209, 112864.
- (5) Khalid, M. Y.; Arif, Z. U.; Noroozi, R.; Hossain, M.; Ramakrishna, S.; Umer, R. 3D/4D Printing of Cellulose Nanocrystals-Based Biomaterials: Additives for Sustainable Applications. *Int. J. Biol. Macromol.* **2023**, 251, 126287.
- (6) Jiang, X.; Mietner, J. B.; Harder, C.; Komban, R.; Chen, S.; Strelow, C.; Sazama, U.; Fröba, M.; Gimmler, C.; Müller-Buschbaum, P.; Roth, S. V.; Navarro, J. R. G. 3D Printable Hybrid Gel Made of Polymer Surface-Modified Cellulose Nanofibrils Prepared by Surface-Initiated Controlled Radical Polymerization (SI-SET-LRP) and Upconversion Luminescent Nanoparticles. ACS Appl. Mater. Interfaces 2023, 15 (4), 5687–5700.
- (7) Jiang, X.; Mietner, J. B.; Raveendran, D.; Ovchinnikov, K. V.; Sochor, B.; Mueller, S.; Boehm-Sturm, P.; Lerouge, F.; Chaput, F.; Gurikov, P.; Roth, S. V.; Navarro, J. R. G. Multifunctional Cellulose Nanofibrils—GdF 3 Nanoparticles Hybrid Gel and Its Potential Uses for Drug Delivery and Magnetic Resonance Imaging. *ACS Appl. Nano Mater.* 2023, 6 (22), 21182–21193.
- (8) Huang, R.; Qi, W.; Feng, L.; Su, R.; He, Z. Self-Assembling Peptide—Polysaccharide Hybrid Hydrogel as a Potential Carrier for Drug Delivery. *Soft Matter* **2011**, *7* (13), 6222–6230.
- (9) Li, L.; Zheng, R.; Sun, R. Understanding Multicomponent Low Molecular Weight Gels from Gelators to Networks. *J. Adv. Res.* **2025**, 69, 91–106.
- (10) Gong, X.; Branford-White, C.; Tao, L.; Li, S.; Quan, J.; Nie, H.; Zhu, L. Preparation and Characterization of a Novel Sodium Alginate Incorporated Self-Assembled Fmoc-FF Composite Hydrogel. *Mater. Sci. Eng., C* **2016**, *58*, 478–486.
- (11) Vitale, M.; Ligorio, C.; McAvan, B.; Hodson, N. W.; Allan, C.; Richardson, S. M.; Hoyland, J. A.; Bella, J. Hydroxyapatite-Decorated Fmoc-Hydrogel as a Bone-Mimicking Substrate for Osteoclast Differentiation and Culture. *Acta Biomater.* **2022**, *138*, 144–154.
- (12) Rosa, E.; Diaferia, C.; Gallo, E.; Morelli, G.; Accardo, A. Stable Formulations of Peptide-Based Nanogels. *Molecules* **2020**, 25 (15), 3455.
- (13) Diaferia, C.; Rosa, E.; Morelli, G.; Accardo, A. Fmoc-Diphenylalanine Hydrogels: Optimization of Preparation Methods and Structural Insights. *Pharmaceuticals* **2022**, *15* (9), 1048.
- (14) Lingenfelder, M.; Tomba, G.; Costantini, G.; Colombi Ciacchi, L.; De Vita, A.; Kern, K. Tracking the Chiral Recognition of Adsorbed Dipeptides at the Single-Molecule Level. *Angew. Chem., Int. Ed.* **2007**, 46 (24), 4492–4495.
- (15) Dalloul, F.; Mietner, J. B.; Raveendran, D.; Chen, S.; Barba, E.; Möck, D. M. J.; Hubel, F.; Sochor, B.; Koyiloth Vayalil, S.; Hesse, L.; Olbrich, A.; Appelt, J.; Müller-Buschbaum, P.; Roth, S. V.; Navarro, J. R. G. From Unprintable Peptidic Gel to Unstoppable: Transforming Diphenylalanine Peptide (Fmoc-FF) Nanowires and Cellulose Nanofibrils into a High-Performance Biobased Gel for 3D Printing. ACS Appl. Bio Mater. 2025, 8 (3), 2323–2339.
- (16) Tang, C.; Smith, A. M.; Collins, R. F.; Ulijn, R. V.; Saiani, A. Fmoc-Diphenylalanine Self-Assembly Mechanism Induces Apparent p K a Shifts. *Langmuir* **2009**, *25* (16), 9447–9453.
- (17) Tao, K.; Levin, A.; Adler-Abramovich, L.; Gazit, E. Fmoc-Modified Amino Acids and Short Peptides: Simple Bio-Inspired Building Blocks for the Fabrication of Functional Materials. *Chem. Soc. Rev.* **2016**, 45 (14), 3935–3953.
- (18) Rosa, E.; Diaferia, C.; Gianolio, E.; Sibillano, T.; Gallo, E.; Smaldone, G.; Stornaiuolo, M.; Giannini, C.; Morelli, G.; Accardo, A. Multicomponent Hydrogel Matrices of Fmoc-FF and Cationic Peptides for Application in Tissue Engineering. *Macromol. Biosci.* **2022**, 22 (7), 2200128.
- (19) Diaferia, C.; Morelli, G.; Accardo, A. Fmoc-Diphenylalanine as a Suitable Building Block for the Preparation of Hybrid Materials and Their Potential Applications. *J. Mater. Chem. B* **2019**, 7 (34), 5142–5155.

- (20) Ryu, J.; Park, C. B. High-Temperature Self-Assembly of Peptides into Vertically Well-Aligned Nanowires by Aniline Vapor. *Adv. Mater.* **2008**, *20* (19), 3754–3758.
- (21) Almohammed, S.; Kanoun, M. B.; Goumri-Said, S.; Alam, M. W.; Fularz, A.; Alnaim, A.; Rice, J. H.; Rodriguez, B. J. Thermally-controlled Spherical Peptide Gel Architectures Prepared Using the PH Switch Method. *Pept. Sci.* **2023**, *115* (3), No. e24304.
- (22) Reches, M.; Gazit, E. Controlled Patterning of Aligned Self-Assembled Peptide Nanotubes. *Nat. Nanotechnol.* **2006**, *1* (3), 195–200.
- (23) Lin, Y.; Qiao, Y.; Tang, P.; Li, Z.; Huang, J. Controllable Self-Assembled Laminated Nanoribbons from Dipeptide-Amphiphile Bearing Azobenzene Moiety. *Soft Matter* **2011**, *7* (6), 2762.
- (24) Raeburn, J.; Pont, G.; Chen, L.; Cesbron, Y.; Lévy, R.; Adams, D. J. Fmoc-Diphenylalanine Hydrogels: Understanding the Variability in Reported Mechanical Properties. *Soft Matter* **2012**, 8 (4), 1168–1174.
- (25) Nolan, M. C.; Fuentes Caparrós, A. M.; Dietrich, B.; Barrow, M.; Cross, E. R.; Bleuel, M.; King, S. M.; Adams, D. J. Optimising Low Molecular Weight Hydrogels for Automated 3D Printing. *Soft Matter* **2017**, *13* (45), 8426–8432.
- (26) Netti, F.; Aviv, M.; Dan, Y.; Rudnick-Glick, S.; Halperin-Sternfeld, M.; Adler-Abramovich, L. Stabilizing Gelatin-Based Bioinks under Physiological Conditions by Incorporation of Ethylene-Glycol-Conjugated Fmoc-FF Peptides. *Nanoscale* **2022**, *14* (23), 8525–8533.
- (27) Xie, Y.; Zhao, J.; Huang, R.; Qi, W.; Wang, Y.; Su, R.; He, Z. Calcium-Ion-Triggered Co-Assembly of Peptide and Polysaccharide into a Hybrid Hydrogel for Drug Delivery. *Nanoscale Res. Lett.* **2016**, *11* (1), 184.
- (28) Ghosh, M.; Halperin-Sternfeld, M.; Grinberg, I.; Adler-Abramovich, L. Injectable Alginate-Peptide Composite Hydrogel as a Scaffold for Bone Tissue Regeneration. *Nanomaterials* **2019**, 9 (4), 497.
- (29) Curvello, R.; Raghuwanshi, V. S.; Garnier, G. Engineering Nanocellulose Hydrogels for Biomedical Applications. *Adv. Colloid Interface Sci.* **2019**, 267, 47–61.
- (30) Das, S.; Ghosh, B.; Sarkar, K. Nanocellulose as Sustainable Biomaterials for Drug Delivery. *Sens. Int.* **2022**, *3*, 100135.
- (31) Huang, L.; Yuan, W.; Hong, Y.; Fan, S.; Yao, X.; Ren, T.; Song, L.; Yang, G.; Zhang, Y. 3D Printed Hydrogels with Oxidized Cellulose Nanofibers and Silk Fibroin for the Proliferation of Lung Epithelial Stem Cells. *Cellulose* **2021**, 28 (1), 241–257.
- (32) Battisto, E. W.; Sarsfield, S. R.; Lele, S. R.; Williams, T.; Catchmark, J. M.; Chmely, S. C. Enhancing the Matrix—Fiber Interface with a Surfactant Leads to Improved Performance Properties of 3D Printed Composite Materials Containing Cellulose Nanofibrils. ACS Appl. Mater. Interfaces 2022, 14 (39), 44841—44848.
- (33) Wang, X.; Wang, Q.; Xu, C. Nanocellulose-Based Inks for 3D Bioprinting: Key Aspects in Research Development and Challenging Perspectives in Applications—A Mini Review. *Bioengineering* **2020**, 7
- (34) Quan, L.; Xin, Y.; Wu, X.; Ao, Q. Mechanism of Self-Healing Hydrogels and Application in Tissue Engineering. *Polymers (Basel)* **2022**, *14* (11), 2184.
- (35) Mietner, J. B.; Jiang, X.; Edlund, U.; Saake, B.; Navarro, J. R. G. 3D Printing of a Bio-Based Ink Made of Cross-Linked Cellulose Nanofibrils with Various Metal Cations. *Sci. Rep.* **2021**, *11* (1), 6461.
- (36) Syrový, T.; Maronová, S.; Kuberský, P.; Ehman, N. V.; Vallejos, M. E.; Pretl, S.; Felissia, F. E.; Area, M. C.; Chinga-Carrasco, G. Wide Range Humidity Sensors Printed on Biocomposite Films of Cellulose Nanofibril and Poly(Ethylene Glycol). *J. Appl. Polym. Sci.* **2019**, *136* (36), 47920.
- (37) Milne, S. D.; Seoudi, I.; Al Hamad, H.; Talal, T. K.; Anoop, A. A.; Allahverdi, N.; Zakaria, Z.; Menzies, R.; Connolly, P. A Wearable Wound Moisture Sensor as an Indicator for Wound Dressing Change: An Observational Study of Wound Moisture and Status. *Int. Wound J.* **2016**, *13* (6), 1309–1314.
- (38) Chinga-Carrasco, G. Potential and Limitations of Nanocelluloses as Components in Biocomposite Inks for Three-Dimensional Bioprinting and for Biomedical Devices. *Biomacromolecules* **2018**, *19* (3), 701–711.

- (39) Dong, H.; Snyder, J. F.; Williams, K. S.; Andzelm, J. W. Cation-Induced Hydrogels of Cellulose Nanofibrils with Tunable Moduli. *Biomacromolecules* **2013**, *14* (9), 3338–3345.
- (40) Mittal, N.; Jansson, R.; Widhe, M.; Benselfelt, T.; Håkansson, K. M. O.; Lundell, F.; Hedhammar, M.; Söderberg, L. D. Ultrastrong and Bioactive Nanostructured Bio-Based Composites. *ACS Nano* **2017**, *11* (5), 5148–5159.
- (41) Masruchin, N.; Park, B.-D.; Causin, V.; Um, I. C. Characteristics of TEMPO-Oxidized Cellulose Fibril-Based Hydrogels Induced by Cationic Ions and Their Properties. *Cellulose* **2015**, 22 (3), 1993–2010.
- (42) Onyianta, A. J.; Castellano, M.; Dorris, M.; Williams, R. L.; Vicini, S. The Effects of Morpholine Pre-Treated and Carboxymethylated Cellulose Nanofibrils on the Properties of Alginate-Based Hydrogels. *Carbohydr. Polym.* **2018**, *198*, 320–327.
- (43) Rossetti, A.; Paciaroni, A.; Rossi, B.; Bottari, C.; Comez, L.; Corezzi, S.; Melone, L.; Almásy, L.; Punta, C.; Fiorati, A. TEMPO-Oxidized Cellulose Nanofibril/Polyvalent Cations Hydrogels: A Multifaceted View of Network Interactions and Inner Structure. *Cellulose* 2023, 30 (5), 2951–2967.
- (44) Fiorati, A.; Contessi Negrini, N.; Baschenis, E.; Altomare, L.; Faré, S.; Giacometti Schieroni, A.; Piovani, D.; Mendichi, R.; Ferro, M.; Castiglione, F.; Mele, A.; Punta, C.; Melone, L. TEMPO-Nanocellulose/Ca2+ Hydrogels: Ibuprofen Drug Diffusion and In Vitro Cytocompatibility. *Materials (Basel)* **2020**, *13* (1), 183.
- (45) Dalloul, F.; Mietner, J. B.; Navarro, J. R. G. Three-Dimensional Printing of a Tough Polymer Composite Gel Ink Reinforced with Chemically Modified Cellulose Nanofibrils Showing Self-Healing Behavior. *ACS Appl. Polym. Mater.* **2023**, *5* (5), 3256–3269.
- (46) Shinoda, R.; Saito, T.; Okita, Y.; Isogai, A. Relationship between Length and Degree of Polymerization of TEMPO-Oxidized Cellulose Nanofibrils. *Biomacromolecules* **2012**, *13* (3), 842–849.
- (47) Buffet, A.; Rothkirch, A.; Döhrmann, R.; Körstgens, V.; Abul Kashem, M. M.; Perlich, J.; Herzog, G.; Schwartzkopf, M.; Gehrke, R.; Müller-Buschbaum, P.; Roth, S. V. P03, the Microfocus and Nanofocus X-Ray Scattering (MiNaXS) BeamLine of the PETRA III Storage Ring: The Microfocus Endstation. *J. Synchrotron Radiat.* **2012**, *19* (4), 647–653.
- (48) Fukuzumi, H.; Tanaka, R.; Saito, T.; Isogai, A. Dispersion Stability and Aggregation Behavior of TEMPO-Oxidized Cellulose Nanofibrils in Water as a Function of Salt Addition. *Cellulose* **2014**, *21* (3), 1553–1559.
- (49) Ono, Y.; Fukui, S.; Funahashi, R.; Isogai, A. Relationship of Distribution of Carboxy Groups to Molar Mass Distribution of TEMPO-Oxidized Algal, Cotton, and Wood Cellulose Nanofibrils. *Biomacromolecules* **2019**, 20 (10), 4026–4034.
- (50) Smith, A. M.; Williams, R. J.; Tang, C.; Coppo, P.; Collins, R. F.; Turner, M. L.; Saiani, A.; Ulijn, R. V. Fmoc-Diphenylalanine Self Assembles to a Hydrogel via a Novel Architecture Based on $\pi \pi$ Interlocked β -Sheets. *Adv. Mater.* **2008**, 20 (1), 37–41.
- (51) Ee, L. Y.; Yau Li, S. F. Recent Advances in 3D Printing of Nanocellulose: Structure, Preparation, and Application Prospects. *Nanoscale Adv.* **2021**, 3 (5), 1167–1208.
- (52) Isogai, A.; Saito, T.; Fukuzumi, H. TEMPO-Oxidized Cellulose Nanofibers. *Nanoscale* **2011**, 3 (1), 71–85.
- (53) Solhi, L.; Guccini, V.; Heise, K.; Solala, I.; Niinivaara, E.; Xu, W.; Mihhels, K.; Kröger, M.; Meng, Z.; Wohlert, J.; Tao, H.; Cranston, E. D.; Kontturi, E. Understanding Nanocellulose—Water Interactions: Turning a Detriment into an Asset. *Chem. Rev.* **2023**, *123* (5), 1925—2015.
- (54) Madivoli, E. S.; Schwarte, J. V.; Kareru, P. G.; Gachanja, A. N.; Fromm, K. M. Stimuli-Responsive and Antibacterial Cellulose-Chitosan Hydrogels Containing Polydiacetylene Nanosheets. *Polymers* (*Basel*) 2023, 15 (5), 1062.
- (55) Paxton, N.; Smolan, W.; Böck, T.; Melchels, F.; Groll, J.; Jungst, T. Proposal to Assess Printability of Bioinks for Extrusion-Based Bioprinting and Evaluation of Rheological Properties Governing Bioprintability. *Biofabrication* **2017**, 9 (4), 044107.
- (56) Xu, J.; Zhou, Z.; Cai, J.; Tian, J. Conductive Biomass-Based Composite Wires with Cross-Linked Anionic Nanocellulose and

- Cationic Nanochitin as Scaffolds. *Int. J. Biol. Macromol.* **2020**, *156*, 1183–1190.
- (57) Hughes, E.; O'Neill, N. S.; Schweitzer-Stenner, R. Ordered Aggregates of Fmoc-Diphenylalanine at Alkaline PH as a Precursor of Fibril Formation and Peptide Gelation. *J. Phys. Chem. B* **2025**, *129* (1), 260–272.
- (58) Österberg, M.; Henn, K. A.; Farooq, M.; Valle-Delgado, J. J. Biobased Nanomaterials—The Role of Interfacial Interactions for Advanced Materials. *Chem. Rev.* **2023**, *123* (5), 2200–2241.
- (59) Escobar, I. C.; Randall, A. A.; Hong, S. K.; Taylor, J. S. Effect of Solution Chemistry on Assimilable Organic Carbon Removal by Nanofiltration: Full and Bench Scale Evaluation. *J. Water Supply:Res. Technol.*—AQUA 2002, 51 (2), 67—76.
- (60) Ravindran, L.; Sreekala, M. S.; Thomas, S. Novel Processing Parameters for the Extraction of Cellulose Nanofibres (CNF) from Environmentally Benign Pineapple Leaf Fibres (PALF): Structure-Property Relationships. *Int. J. Biol. Macromol.* **2019**, *131*, 858–870.
- (61) Fiorati, A.; Baldassarre, F.; Riva, L.; Tacconi, S.; Nobile, C.; Vergaro, V.; Grisorio, R.; Melone, L.; Mele, A.; Dini, L.; Punta, C.; Ciccarella, G. Synthesis of Microsponges by Spray Drying TEMPO-Oxidized Cellulose Nanofibers and Characterization for Controlled Release. J. Drug Delivery Sci. Technol. 2023, 89, 105080.
- (62) Nissilä, T.; Wei, J.; Geng, S.; Teleman, A.; Oksman, K. Ice-Templated Cellulose Nanofiber Filaments as a Reinforcement Material in Epoxy Composites. *Nanomaterials* **2021**, *11* (2), 490.
- (63) Mendoza, L.; Batchelor, W.; Tabor, R. F.; Garnier, G. Gelation Mechanism of Cellulose Nanofibre Gels: A Colloids and Interfacial Perspective. *J. Colloid Interface Sci.* **2018**, *509*, 39–46.
- (64) Xu, C.; Zhang Molino, B.; Wang, X.; Cheng, F.; Xu, W.; Molino, P.; Bacher, M.; Su, D.; Rosenau, T.; Willför, S.; Wallace, G. 3D Printing of Nanocellulose Hydrogel Scaffolds with Tunable Mechanical Strength towards Wound Healing Application. *J. Mater. Chem. B* **2018**, *6* (43), 7066–7075.
- (65) Panja, S.; Adams, D. J. Maintaining Homogeneity during a Sol—Gel Transition by an Autocatalytic Enzyme Reaction. *Chem. Commun.* **2019**, *55* (1), 47–50.
- (66) Cohen, D. L.; Lo, W.; Tsavaris, A.; Peng, D.; Lipson, H.; Bonassar, L. J. Increased Mixing Improves Hydrogel Homogeneity and Quality of Three-Dimensional Printed Constructs. *Tissue Eng., Part C* **2011**, *17* (2), 239–248.
- (67) Truong, W. T.; Su, Y.; Gloria, D.; Braet, F.; Thordarson, P. Dissolution and Degradation of Fmoc-Diphenylalanine Self-Assembled Gels Results in Necrosis at High Concentrations in Vitro. *Biomater. Sci.* **2015**, 3 (2), 298–307.
- (68) Dudukovic, N. A.; Zukoski, C. F. Mechanical Properties of Self-Assembled Fmoc-Diphenylalanine Molecular Gels. *Langmuir* **2014**, *30* (15), 4493–4500.
- (69) Martin, A. D.; Robinson, A. B.; Mason, A. F.; Wojciechowski, J. P.; Thordarson, P. Exceptionally Strong Hydrogels through Self-Assembly of an Indole-Capped Dipeptide. *Chem. Commun.* **2014**, *50* (98), 15541–15544.
- (70) Nguyen, T. H. M.; Abueva, C.; Van Ho, H.; Lee, S.-Y.; Lee, B.-T. In Vitro and in Vivo Acute Response towards Injectable Thermosensitive Chitosan/TEMPO-Oxidized Cellulose Nanofiber Hydrogel. *Carbohydr. Polym.* **2018**, *180*, 246–255.



CAS BIOFINDER DISCOVERY PLATFORM™

BRIDGE BIOLOGY AND CHEMISTRY FOR FASTER ANSWERS

Analyze target relationships, compound effects, and disease pathways

Explore the platform

